NJC

LETTER

View Article Online
View Journal | View Issue

Facile synthesis of hematite nanoparticles and nanocubes and their shape-dependent optical properties

Cite this: *New J. Chem.*, 2014, 38, 46

Received (in Montpellier, France) 5th September 2013, Accepted 10th October 2013

DOI: 10.1039/c3nj01060k

www.rsc.org/njc

Ting Wang,[ab] Shuang Zhou,[c] Caihong Zhang,[c] Jiabiao Lian,*[c] Yao Liang*[d] and Wenxiang Yuan*[a]

Hematite nanoparticles and nanocubes were prepared by a simple hydrolysis of iron(II) acetate, which exhibited interesting shape-dependent optical properties. The simple and low-cost method could be scaled up easily, which may pave the way for the practical applications.

Hematite (α-Fe_2O_3) is the most stable iron oxide with n-type semiconducting properties and has been extensively applied in catalysts,[1–3] pigments,[4] and gas sensors,[5–7] due to its favorable optical band gap (2.2 eV), extraordinary chemical stability in an oxidative environment, abundance, and low cost. Many recent efforts have been directed toward the fabrication of iron oxide nanostructures to enhance their performance in the current applications. To date, a series of solution-based routes and vapor-phase processes have been used to fabricate iron oxide nanostructures with different dimensionalities.[8–11] However, these synthesis routes involved the introduction of surfactants, high temperatures, and precursor calcination steps and were often time-consuming. For the sake of practicality, it is desirable to develop a facile and environmentally friendly route to synthesize the hematite nanostructures.

One of the most fascinating and useful aspects of metal oxide nanomaterials is their optical properties. Applications based on their optical properties include optical detection, imaging, photocatalysis, and solar cells.[12–15] The optical properties of nanomaterials strongly depend on parameters such as feature size, shape, surface characteristics, and doping.[16–20] Likewise, shape can have a dramatic influence on the optical properties of nanostructures. For example, the apparent color of hematite nanocrystals could be changed from bloody brown to dark brown, due to the reason that some specific surface planes possess a higher reflectance ability than other surface planes.[21]

Here we report a facile and environmentally benign green route to synthesize hematite nanostructures *via* a simple hydrolysis of iron(II) acetate. The most intriguing feature of this approach is that it is very simple and can be employed in large-scale production. Only one reactant $Fe(CH_3COO)_2{\cdot}4H_2O$ is used, neither templates nor other additives are required in the reaction system. The precursor not only serves as an iron source, but also provides an effective etchant CH_3COOH. Moreover, their shape-dependent optical properties are also investigated.

The purity and crystallinity of the as-prepared samples were examined using powder XRD measurements (Fig. 1). Fig. 1a and b show the XRD patterns of the as-prepared S-1 and S-2, respectively. It is evident that all the peaks can be indexed to the hexagonal structure of α-Fe_2O_3 [space group: $R\bar{3}c$, (167),

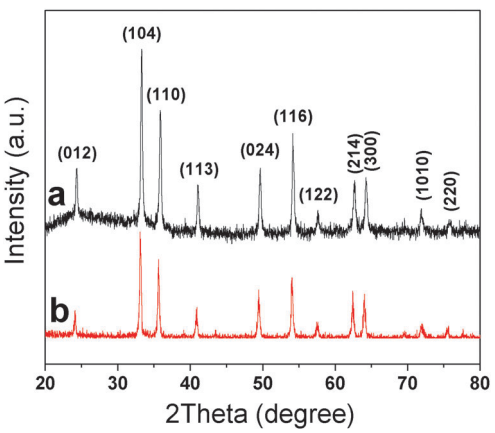

Fig. 1 XRD patterns of the as-synthesized α-Fe_2O_3 nanoparticles (a) and nanocubes (b).

[a] *Shenzhen Key Laboratory of New Lithium-Ion Battery and Mesoporous Materials, College of Chemistry and Chemical Engineering, Shenzhen University, Shenzhen 518060, Guangdong, P. R. China. E-mail: wxyuanster@gmail.com*
[b] *School of Environmental Science and Engineering, Fujian Normal University, Fuzhou 350007, Fujian, P. R. China*
[c] *Department of Electronic Engineering, The Chinese University of Hong Kong, Hong Kong, P. R. China. E-mail: jblian@phy.cuhk.edu.hk; Tel: +852-67341261*
[d] *School of Materials Science and Engineering, Dalian Jiaotong University, Dalian 116028, Liaoning, P. R. China. E-mail: liangyao@djtu.edu.cn*

JCPDS Card 79-1741]. No other peaks are observed, indicating the high purity of the as-prepared samples. The average crystallite size of the S-1 and S-2 could be calculated to be about 33.2 and 29.6 nm, respectively, on the basis of the full width at half maximum (FWHM) of the (104) diffraction peak using the Scherrer formula.

$$D_{hkl} = K\,\lambda/(B_{hkl}\cos\theta_{hkl})$$

where D_{hkl} is the particle size perpendicular to the normal line of the (hkl) plane, K is a constant (it is 0.9), B_{hkl} is the full width at half-maximum of the (hkl) diffraction peak, θ_{hkl} is Bragg's angle of the (hkl) peak, and λ is the wavelength of X-ray.

Fig. 2a shows the low-magnification FE-SEM image of sample S-1, which is composed of uniform monodispersed nanoparticles. The high-magnification FE-SEM image (Fig. 2b) indicates that the surface of the nanoparticles is relatively rough. The corresponding TEM image (Fig. 3a) further demonstrates that the obtained nanoparticles have homogeneous size with a diameter of about 35 nm, which is consistent with that calculated from Scherrer's formula. The high-magnification TEM image (Fig. 3b) gives further evidence for the rough surface of the as-prepared nanoparticles. The morphology of the α-Fe_2O_3 nanocubes (S-2) with highly geometrical symmetry was visualized by FE-SEM and TEM. The typical low-magnification FE-SEM image (Fig. 2c) clearly shows that the product possesses a large-scale uniform size. The high-magnification FE-SEM image (Fig. 2d) displays that the sample has a cubic structure and the surfaces of the nanocubes are also relatively rough. The corresponding TEM (Fig. 3c and d) images further indicate that the as-prepared S-2 sample has a well-defined cubic shape and the size of the nanocubes is about 30 nm at edges.

The rough surfaces of the as-prepared samples are probably due to the etching effect of CH_3COOH generated during the reaction. As reported in our previous work,[18,22] the possible reaction mechanism is illustrated as follows:

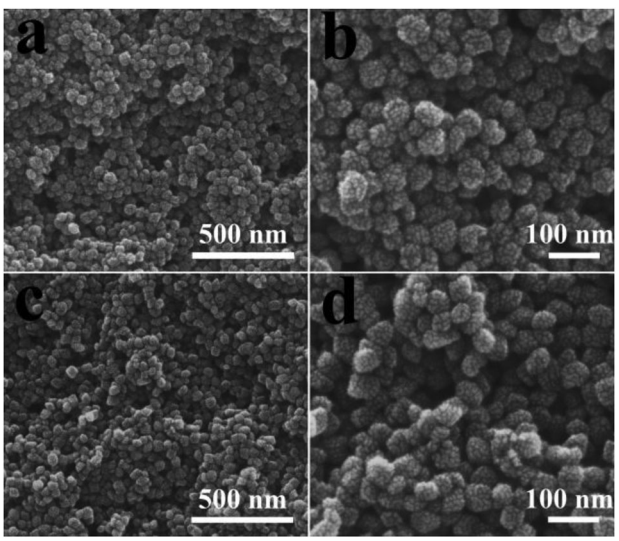

Fig. 2 (a and c) Low- and (b and d) high-magnification FE-SEM images of the as-synthesized α-Fe_2O_3 nanoparticles and nanocubes, respectively.

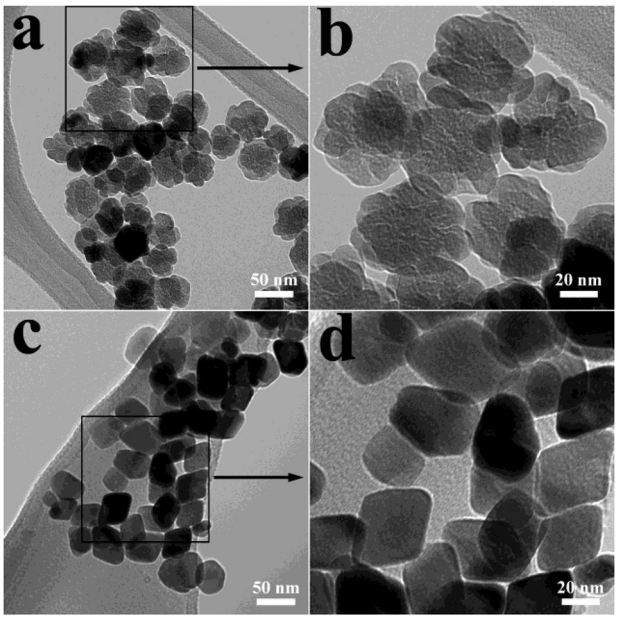

Fig. 3 (a and c) Low- and (b and d) high-magnification TEM images of the as-synthesized α-Fe_2O_3 nanoparticles and nanocubes, respectively.

$$CH_3COO^- + H_2O \leftrightarrow CH_3COOH + OH^- \quad (1)$$

$$4Fe^{2+} + 8OH^- + O_2 \rightarrow 4Fe(OH)_3/FeOOH \xrightarrow[\text{Condition}]{\text{Hydrothermal}} \alpha\text{-}Fe_2O_3 \quad (2)$$

$$\alpha\text{-}Fe_2O_3 + 6CH_3COOH \leftrightarrow 2Fe^{3+} + 6CH_3COO^- + 3H_2O \quad (3)$$

As shown above, Fe^{3+} reacted with OH^- (produced by the hydrolysis of CH_3COO^-, eqn (1)) and O_2 in air to form a $Fe(OH)_3$ or FeOOH suspension, which was easily dehydrated under further hydrothermal conditions to form α-Fe_2O_3 [eqn (2)]. As the reaction proceeded, more and more CH_3COOH was generated to form an acidic solution, in which the surfaces of the products were easily attacked by the protons [eqn (3)] and consequently became rough.

The optical properties of the as-prepared α-Fe_2O_3 samples were investigated at room temperature by UV-vis spectroscopy. Fig. 4a shows the optical absorption spectrum of the as-synthesized α-Fe_2O_3 nanoparticles, which shows an intense peak at 240 nm and a broad hump-like shoulder in the wavelength region of 350–550 nm. For the α-Fe_2O_3 nanocubes (Fig. 4b), the absorption band is mainly located in the ultraviolet region, with an intense peak at 239 nm and a broad band from 280 to 400 nm, which is different from that of nanoparticles, due to the change in the degree of transition depending on the shape of the samples.

It has been demonstrated that the absorption bands in the ultraviolet region from 200 to 400 nm are attributed to the ligand-to-metal charge transfer (direct transitions) and partly from the contributions of the Fe^{3+} ligand field transition $^6A_1 \rightarrow {}^4T_1(^4P)$ at 290–310 nm, $^6A_1 \rightarrow {}^4E(^4D)$ and $^6A_1 \rightarrow {}^4T_2(^4D)$ at 360–380 nm, and $^6A_1 \rightarrow {}^4E(^4G)$ at 390 nm. The visible region (400–600 nm) is assigned to the pair excitation processes $^6A_1 + {}^6A_1$ to $^4T_1(^4G) + {}^4T_1(^4G)$ at 485–550 nm, and is most likely

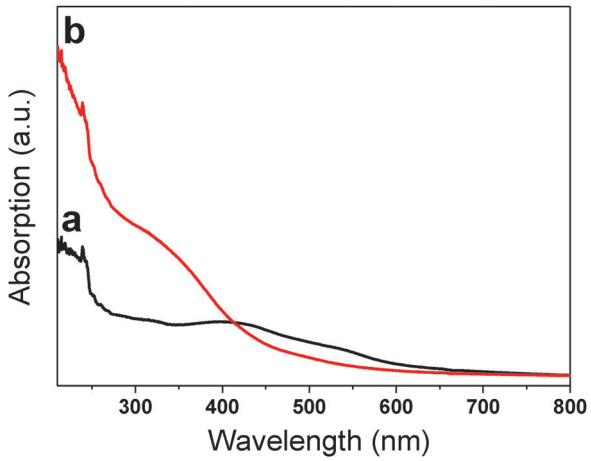

Fig. 4 The shape-dependent UV-vis spectra of the as-synthesized α-Fe_2O_3 nanoparticles (a) and nanocubes (b).

overlapped by the contributions of $^6A_1 \rightarrow {}^4E$, $^4A_1(^4G)$ ligand field transitions of Fe^{3+} at 430 nm.[18,23–25] As revealed from Fig. 4, the pair excitation processes as well as the ligand field transitions of Fe^{3+} at 430 nm dominate for the optical absorption features of the nanoparticles, while the electronic transition for the charge transfer in the wavelength region 210–400 nm dominates for the optical absorption features of the nanocubes. The results indicate that the shape of the samples can change the degree of transition.

In summary, the α-Fe_2O_3 nanoparticles and nanocubes have been synthesized *via* a facile hydrothermal method. The etching process (the effect of CH_3COOH generated from the reaction) is of critical importance for the formation of the rough surface. The present synthesis method is much easier, which is critical for large-scale production and future practical applications. Investigations of UV-vis spectra of the as-prepared samples provide evidence for their shape-dependent optical properties. Moreover, the hematite nanostructures with broad absorption in the ultraviolet region from the electron transmission of Fe–O are expected to be used as ultraviolet ray absorbents.

Experimental

All the reagents were of analytical grade and used without further purification. In a typical synthesis procedure, 1.5 mmol of $Fe(CH_3COO)_2{\cdot}4H_2O$ was put into 30 mL of deionized water or 30 mL mixed solution of deionized water and anhydrous ethanol with a volume ratio of 15 : 15. The samples were labeled as S-1 and S-2, respectively. Each mixture was stirred for 20 min to form a homogeneous solution before it was transferred to a stainless-steel autoclave, sealed and heated at 150 °C for 12 h. When the reaction was completed, the autoclave was naturally cooled to room temperature. The resultant product was collected and washed with deionized water and anhydrous ethanol several times until the solution was neutral. The final red product was dried in a vacuum at 80 °C for 3 h.

X-ray diffraction (XRD) measurements were conducted on a Rigaku RU300 diffractometer using Cu K_α radiation (λ = 0.154 nm) at V = 40 kV and I = 40 mA. The scanning speed was set at 3° min^{-1}. Morphology observation was performed on a Quanta F400 field emission scanning electron microscope (FE-SEM). Transmission electron microscopy (TEM) images were recorded using a Tecnai G^2 20S-Twin transmission electron microscope operating at an accelerating voltage of 120 kV. The ultraviolet-visible spectrum was obtained from powders suspended in anhydrous ethanol using a Hitachi UV-visible recording spectrophotometer (U-3501) between 210 and 800 nm.

Acknowledgements

This work was financially supported by the Science and Technology Innovation Commission of Shenzhen (Project No. JCYJ20120817163755065) and the National Natural Science Foundation of China (Grant No. 61204016).

Notes and references

1 I. Cesar, A. Kay, J. A. G. Martinez and M. Gratzel, *J. Am. Chem. Soc.*, 2006, **128**, 4582–4583.
2 Y. Ling, G. Wang, D. A. Wheeler, J. Z. Zhang and Y. Li, *Nano Lett.*, 2011, **11**, 2119–2125.
3 A. Kay, I. Cesar and M. Gratzel, *J. Am. Chem. Soc.*, 2006, **128**, 15714–15721.
4 H. Katsuki and S. Komarneni, *J. Am. Ceram. Soc.*, 2003, **86**, 183–185.
5 J. Chen, L. N. Xu, W. Y. Li and X. L. Gou, *Adv. Mater.*, 2005, **17**, 582–587.
6 Z. Y. Sun, H. Q. Yuan, Z. M. Liu, B. X. Han and X. R. Zhang, *Adv. Mater.*, 2005, **17**, 2993–2996.
7 X. J. Liu, Z. Chang, L. Luo, X. D. Lei, J. F. Liu and X. M. Sun, *J. Mater. Chem.*, 2012, **22**, 7232–7238.
8 J. M. Ma, J. B. Lian, X. C. Duan, X. D. Liu and W. J. Zheng, *J. Phys. Chem. C*, 2010, **114**, 10671–10676.
9 J. M. Ma, T. H. Wang, X. C. Duan, J. B. Lian, Z. F. Liu and W. J. Zheng, *Nanoscale*, 2011, **3**, 4372–4375.
10 B. Wang, J. S. Chen, H. B. Wu, Z. Y. Wang and X. W. Lou, *J. Am. Chem. Soc.*, 2011, **133**, 17146–17148.
11 A. Kay, I. Cesar and M. Gratzel, *J. Am. Chem. Soc.*, 2006, **128**, 15714–15721.
12 J. Li and J. Z. Zhang, *Coord. Chem. Rev.*, 2009, **253**, 3015–3041.
13 L. C. He, Y. S. Xiong, M. T. Zhao, X. Mao, Y. L. Liu, H. J. Zhao and Z. Y. Tang, *Chem.–Asian J.*, 2013, **8**, 1765–1767.
14 L. Liu, L. Fu, Y. Liu, Y. L. Liu, P. Jiang, S. Q. Liu, M. Y. Gao and Z. Y. Tang, *Cryst. Growth Des.*, 2009, **9**, 4793–4796.
15 A. Kongkanand, K. Tvrdy, K. Takechi, M. Kuno and P. V. Kamat, *J. Am. Chem. Soc.*, 2008, **130**, 4007–4015.
16 J. B. Lian, Y. Liang, F. L. Kwong, Z. M. Ding and D. H. L. Ng, *Mater. Lett.*, 2012, **66**, 318–320.
17 C. Burda, X. Chen, R. Narayanan and M. A. El-Sayed, *Chem. Rev.*, 2005, **105**, 1025–1102.
18 J. B. Lian, X. C. Duan, J. M. Ma, P. Peng, T. Kim and W. J. Zheng, *ACS Nano*, 2009, **3**(11), 3749–3761.
19 C. H. Hung and W. T. Whang, *J. Mater. Chem.*, 2005, **15**, 267–274.

20 J. B. Lian, C. H. Zhang, Q. Li and D. H. L. Ng, *Nanoscale*, 2013, DOI: 10.1039/c3nr03019a.
21 L. Chen, X. Yang, J. Chen, J. Liu, H. Wu, H. Zhan, C. Liang and M. Wu, *Inorg. Chem.*, 2010, **49**, 8411–8420.
22 J. B. Lian, Z. M. Ding, F. L. Kwong and D. H. L. Ng, *CrystEngComm*, 2011, **13**, 4820–4822.
23 L. A. Marusak, R. Messier and W. B. White, *J. Phys. Chem. Solids*, 1980, **41**, 981–984.
24 D. M. Sherman and T. D. Waite, *Am. Mineral.*, 1985, **70**, 1262–1269.
25 D. A. Wheeler, G. M. Wang, Y. C. Ling, Y. Li and J. Z. Zhang, *Energy Environ. Sci.*, 2012, **5**, 6682–6702.